Title: Stretchable pumps for soft machines

Author's Accepted Manuscript version of

Cacucciolo V, Shintake J, Kuwajima Y, Maeda S, Floreano D, Shea H. Stretchable pumps for soft machines. Nature. 2019 Aug; 572(7770):516–9.

DOI: 10.1038/s41586-019-1479-6

URL : https://www.nature.com/articles/s41586-019-1479-6

Authors: Vito Cacucciolo[1]*, Jun Shintake[2,3], Yu Kuwajima[4], Shingo Maeda[4], Dario Floreano[2], Herbert Shea[1]*

Affiliations:

[1]Soft Transducers Laboratory (LMTS), Institute of Microengineering, School of Engineering, École Polytechnique Fédérale de Lausanne (EPFL), Rue de la Maladière 71b, 2000 Neuchâtel, Switzerland.

[2]Laboratory of Intelligent Systems (LIS), Institute of Microengineering, School of Engineering, École Polytechnique Fédérale de Lausanne (EPFL), Route Cantonale, 1015 Lausanne, Switzerland.

[3]Department of Mechanical and Intelligent Systems Engineering, School of Informatics and Engineering, The University of Electro-Communications, 1-5-1 Chofugaoka, Chofu, 182-8585 Tokyo, Japan.

[4]Smart Materials Laboratory, Department of Engineering Science and Mechanics, Shibaura Institute of Technology, 3-7-5 Toyosu, Koto, 135-8548 Tokyo, Japan.

*Correspondence to: vito.cacucciolo@epfl.ch, herbert.shea@epfl.ch

Text:

Machines made of soft materials bridge life sciences and engineering[1]. Advances in soft materials have enabled skin-like sensors and muscle-like actuators for soft robots and wearables[1–3]. Flexible or stretchable counterparts of most key mechatronic components have been developed[4], principally using fluidically-driven systems[5–7], though other mechanisms have been reported[8], including electrostatic[9–12], stimuli responsive gels[13,14], and thermally responsive materials such as liquid metals[15–17] and shape memory polymers[18]. Yet, there exist to date very few soft counterparts of pumps or compressors, greatly limiting the portability and autonomy of soft machines[4,7]. We describe here a class of soft-matter bidirectional pumps based on charge-injection ElectroHydroDynamics (EHD)[19]. These solid-state pumps are flexible, stretchable, modular, scalable, noiseless, and fast. By integrating the pump in a glove, we demonstrate wearable active thermal management. By embedding the pump in an inflatable structure, we report a self-contained fluidic muscle. The stretchable pumps enable the integration of fluidic circuits in any object, paving the way to wearable lab-on-a-chip and microfluidic sensors, thermally active clothing, and autonomous soft robots.

Despite the widespread use of fluidic actuation, there are very few soft counterparts of pumps or compressors. Conventional pumps and compressors are bulky and rigid systems including impellers, bearings, and electrical motors. They often require lubrication and produce noise. Even miniaturized pumps (e.g., based on piezo-actuators or electrophoresis[20]) are rigid and have moving parts with very few exceptions (see Extended Data Table 1). The lack of electrically-powered flexible or stretchable pumps greatly hinders many applications of fluid-driven soft-systems, ranging from robotics and mechatronics (actuators and sensors) to biology (e.g., microfluidics for cell cultures) to wearable devices (heat distribution).

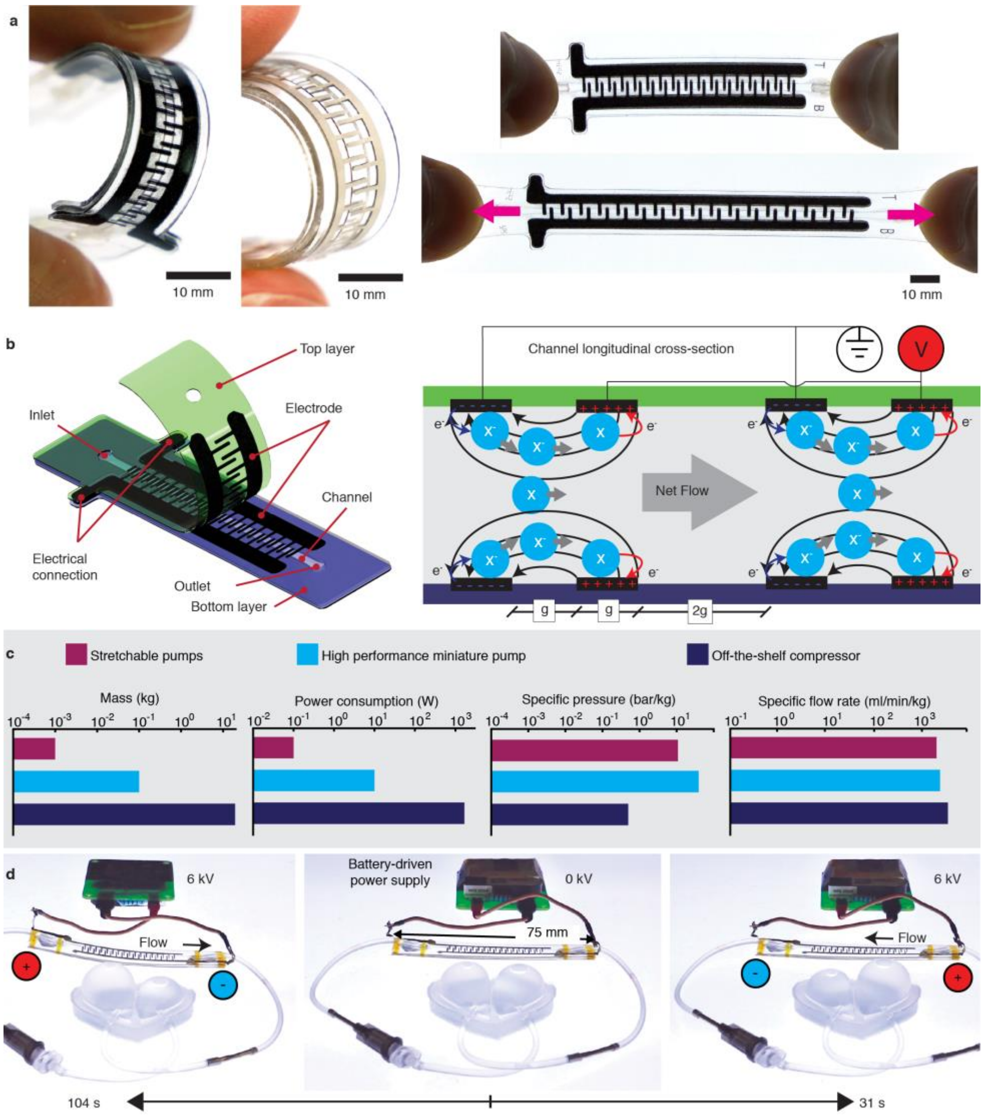

Fig. 1: Stretchable pumps based on charge-injection ElectroHydroDynamics (EHD). a, Pumps made with carbon (left) and silver electrodes (center) bent to a small radius of curvature and stretched to 50% (right). **b left**, Schematic diagram of the stretchable pump. The top and bottom layers are PDMS (Polydimethylsiloxane) membranes of thickness 0.4 mm, on which 30 μm thick compliant electrodes are patterned. The channel is a laser cut 0.5 mm thick PDMS layer. **b right**, Operating principle of the pump. Both top and bottom electrodes are interdigitated. The gap *g* between fingers of opposite polarity is 0.5 mm, and the spacing between finger pairs is 1 mm. The channel is filled with dielectric liquid. When the applied electric field exceeds a threshold of 5 to 8 V/μm, electrons tunnel from the cathode into the liquid. The resulting ions are accelerated by the electric field until they discharge at the anode, dragging neutral liquid along their path, leading to fluid flow. **c**, Performance comparison between the stretchable pumps, a miniature pump (TCS Micropumps, MGD 1000S) and an off-the-shelf compressor (McMaster, single tank portable air compressor) **d**, A demonstration of a stretchable pump moving liquid between two ventricles of a heart-shaped balloon. By changing the polarity of the applied voltage, the flow direction is reversed. The pump is driven by a 20 g battery-operated 6 kV power supply (see Supplementary Video 2).

In this work, we present a class of soft-matter pumps, consisting of a monolithic elastomer tube with embedded compliant electrodes (Fig. 1a, Supplementary Video 1). The pumping mechanism is charge-injection ElectroHydroDynamics (EHD): a dielectric fluid in the channel is accelerated by means of a high DC electric field (6-12 V/µm) (Fig. 1b), allowing pumping in both directions[19,21–25]. See Methods and Extended Data Fig. 1 for a description of the EHD mechanism used in this work. Figure 1c shows a comparison between the stretchable pumps, a high-performance miniature pump (TCS Micropumps, MGD 1000S), and a large off-the-shelf compressor (McMaster, single tank portable air compressor), both commonly used to power soft fluidic actuators[26]. Figure 1d and Supplementary Video 2 show the stretchable pump moving liquid between two ventricles of a heart-shaped balloon, demonstrating bidirectional pumping and high flow-rates. Our solid-state stretchable pumps have no moving parts, are silent, produce no vibration, and operate well when highly bent and even stretched, making them ideal candidates for miniaturization and portability in soft systems.

The modular pumps we developed are compact (75 mm long × 19 mm wide × 1.3 mm thick with a fluidic channel of dimensions 55 mm long × 2 mm wide × 0.5 mm thick), light-weight (1.0 g) and are controlled simply by changing the applied voltage. The pump body material is PDMS (Polydimethylsiloxane) in view of its low Young's modulus, high strain at rupture (>100%), and widespread use in microfluidics. We use established elastomer processing technologies which are highly reproducible and can readily be scaled up for industrial production[27–29]. The cross-section and length of the channel, number of electrodes, and gap between them, can all be easily scaled up or down thanks to our versatile fabrication methods. Extended Data Fig. 2 shows the details of the fabrication process of the pumps, while Extended Data Fig. 3 shows the four generations of pumps that we developed.

Numerous combinations of materials can be implemented for the pump body, electrode, and dielectric liquid, subject to the requirement that the body and electrodes must be stretchable. We focus on two versions that share the same channel geometry and interdigitated electrode design, but with different electrode materials and operating liquids, to illustrate the dependency of pump performance on materials. We refer to the two devices as the “C pump” and “Ag pump” with Carbon- and Silver-based electrodes.

The C pump electrodes are a stretchable composite of carbon black and PDMS, patterned by laser engraving; the fluid is Novec 7100 from 3M. The Ag pump uses a printed stretchable silver ink (Chimet Ag 520 EI) electrodes, and Fluorinert FC-40 from 3M as the dielectric liquid. The Ag devices offer much longer lifetime and higher pressure, but requiring higher voltages than the C pumps. Fluorinert FC-40 is compatible with most elastomers, including PDMS, allowing reliable, long-term operation of the pump. In contrast, Novec 7100 swells PDMS, but is widely used in rigid EHD devices. Ag electrodes enable continuous pumping operation for many hours, while the carbon electrodes have a limited lifetime of order 15 minutes. An advantage of the C pumps is a minimum voltage for pumping that is roughly half that of Ag pumps (2.5 kV vs. 5 kV). However, the Ag pumps can sustain roughly twice the voltage of the C pump (10 kV vs. 6 kV) and can thus generate higher maximum pressure. For the C pump, we measured a generated pressure of over 7 kPa and a maximum flow-rate of over 100 µl/s at 5.6 kV, compared to a maximum pressure of over 14 kPa at 10 kV for the Ag pump. The response time is under one second from zero to maximum pressure for the C pump. The Ag pumps shows in general a slower response. Its performance can be increased by a brief pre-conditioning step at high fields (20 kV/mm).

Figure 2 shows the results of both steady-state and transient characterization experiments. The very low electrical current (1-20 µA) and low power (100 mW) allows powering the pumps by means of miniature batteries and miniaturized DC converters (Extended Data Fig. 4). Flow-rate and pressure values are high enough for macro-scale applications. Additionally, the modular pump elements can be connected in series (Fig. 2F and Extended Data Fig. 5) to increase the output pressure or in parallel to multiply the flow rate. Safe operation on the human body is enabled by using only materials and liquids with very low toxicity and by limiting the electrical current to values far below the human-safety threshold. The intrinsic compliance, low mass, and low power consumption make the soft pumps an enabling tool for portable soft robotics and fluid-based wearable devices. The key performance metrics of our stretchable pumps, including specific pressure, specific flow-rate, and specific power consumption, are comparable to those of published micropumps and commercial pumps, see Fig. 1c and Extended Data Table 1 which contains an overview of pumps operating on a wide range of principles as reviewed in [20,30,31].

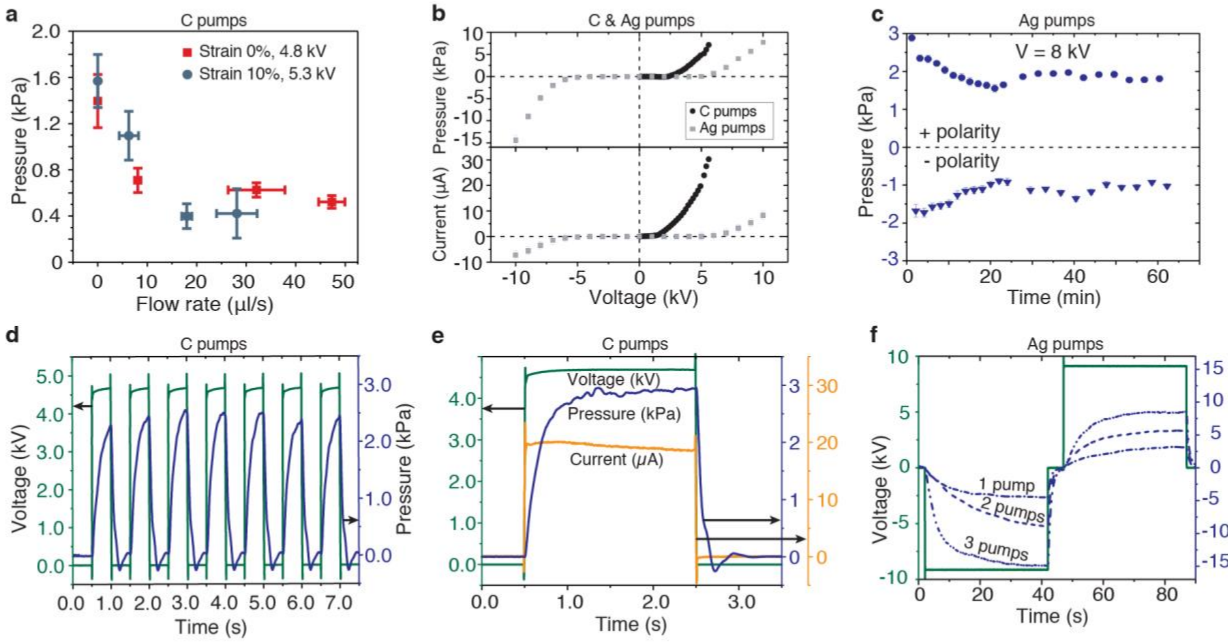

Fig. 2: Performance of the stretchable EHD pumps. a, Pressure vs. flow rate for the C pump at 0% and 10% strain. Error bars represent the standard deviation. The voltage was increased by 10% at 10% strain to keep the same electric field as at 0% strain. **b**, Pressure and electrical current vs. applied voltage, for zero flow-rate (the output valve is closed), for both C and Ag pumps. For the Ag pumps, the flow direction can be reversed by reversing the polarity of the applied voltage. **c**, Lifetime test on the Ag pumps, applying a ± 8kV square wave for one hour. **d**, Pressure generated by the C pump in response to a 1 Hz 0-5kV square wave. **e**, Transient response of the C pumps to a 4.5 kV voltage step, showing a pressure rise time of 0.4 s and a fall time of 0.14 s, both at 10% to 90% pressure. **f**, Pressure generated by three pumps connected in series, when 1, 2 or all the 3 pumps are activated. For the 1 pump and the 2 pumps curves, the data shown are the mean over three experiments, in order to include date from all three devices.

While the C and Ag pumps can both operate at strains of over 50%, we characterized the performance of the C pumps at 0% and 10% applied strain (Fig. 2a) as these strain levels are typical of many soft robotics or wearable applications. The simultaneous measurement of generated flow rate and pressure provides the characteristic curve of the stretchable pumps (Fig. 2b), showing a sub-linear decrease of the pressure as the flow-rate is increased. Performance is nearly unchanged at 10% strain for constant applied electric field. The planar and symmetric electrode design allow the generation of flow in both directions, based on the direction of the applied electric field, as shown in Fig. 2b for the Ag pump, whose pumping direction can be repeatedly reversed. The C pumps can also pump in either direction, but unlike the Ag pumps, the C pumps only operate in the direction in which the field was applied at first operation. Fig. 2c shows a lifetime test of the Ag pump, driven by a bipolar ±8 kV square wave. The period of the square wave is 120 s for the first 25 min and 240 s in the following 35 min. The pumps are undamaged after this experiment, thanks to the very good compatibility between PDMS, the Ag electrodes and the FC-40 dielectric liquid. Fig. 2d-e show the transient response of the C pumps to a 1 Hz unipolar square wave and a 5 kV voltage step. The pressure-voltage response is stable and repeatable. Figure 2f demonstrates pump modularity: three pumps are connected in series (Extended Data Fig. 5) and total pressure is measured when one, two or all the three pumps are activated. The generated pressure scales with the number of active pumps.

There is a large parameter space of electrode configurations and channels geometries that could be explored to further increase performance, see Methods section and Extended Data Fig. 1. The differences between C and Ag pumps indicate that electrode materials and fluid choice play an important role, and offer an avenue to further improve pressure and flow rate.

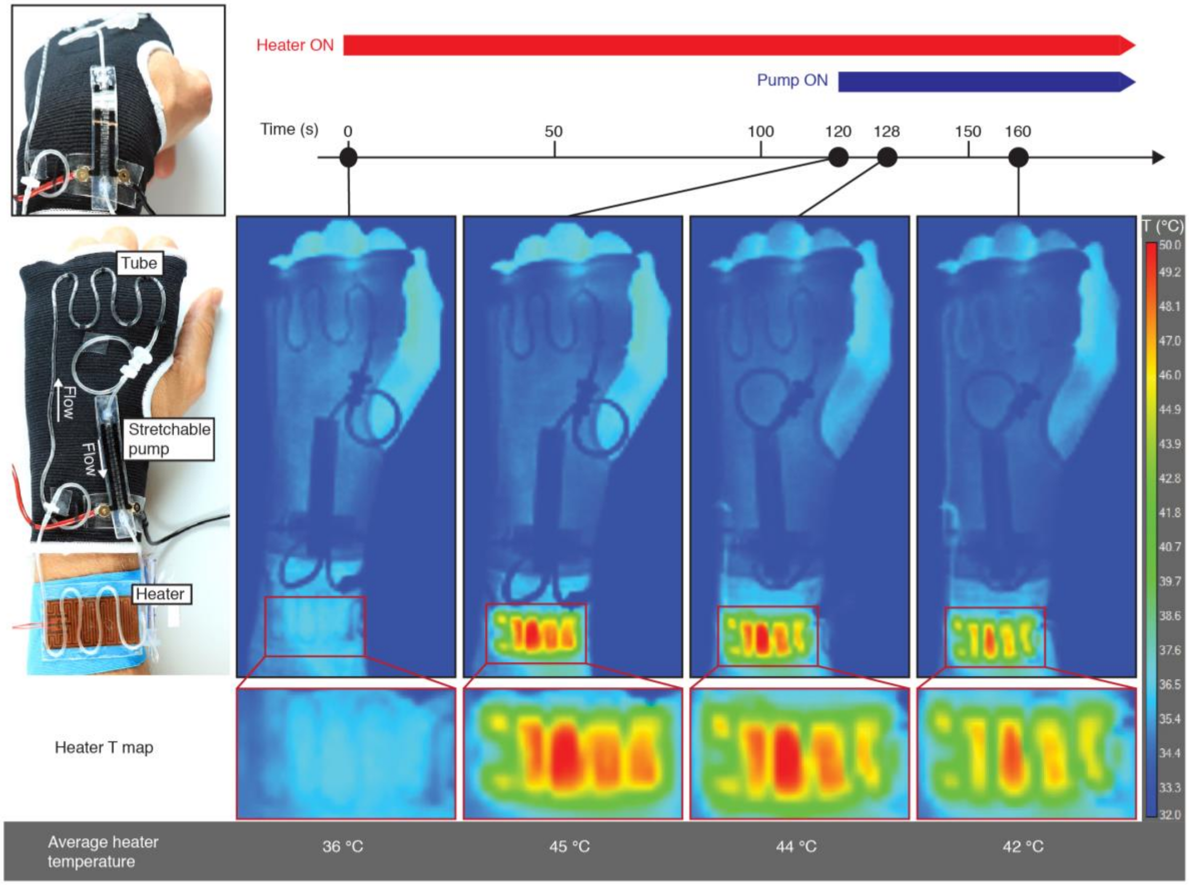

Fig. 3: The stretchable pump is embedded in a textile glove for on-body thermal regulation. The closed loop fluidic circuit consists of the pump and a serpentine flexible tube sewn into the textile glove (the "cold" side), and of a serpentine flexible tube bonded to a flexible heater (the "hot" side). The wearer can easily flex his wrist while the pump is operating. The pump circulates the fluid from the heater to the glove and then back on the opposite side. The colors in the IR images correspond to a temperature map, see colorbar on the far right. The leftmost IR image shows the initial condition when both heater and pump are off. For the second IR image, the heater is on and the pump is off: the temperature at the heater is significantly higher than at the arm. The third IR picture is taken at few seconds after the pump is activated. One can see the cold liquid entering the "hot" circuit from the right tube and the heat being transported away from the left tube. The rightmost IR image shows that the temperature of the heater is significantly decreased after 40 s of fluid circulation. The unchanged temperature of the soft pump confirms its negligible heat generation. Supplementary Video 3 shows the device in action.

We illustrate the broad applicability of the stretchable pumps by demonstrating both a wearable and a soft robotics scenario. In the wearable scenario, the pump is integrated in a textile glove to actively circulate fluid to transport heat between regions on the body (Fig. 3). In the soft robotics scenario, we demonstrate a self-contained fluidic actuator where the pump is embedded in the soft bending structure to move the fluid between two chambers, resulting in large actuation without external fluidic connections (Fig. 4).

For the wearable demonstrator for temperature control (Fig. 3), the pump is integrated in a textile glove and circulates the dielectric fluid from a hot zone, consisting of a membrane heater, to a cooling tubing embedded in the glove. We monitor the temperature of the system using an infrared (IR) camera, which showed that the temperature of the heater was significantly decreased by fluid circulation and that the soft pump did not heat the liquid, thanks to the pump's low power consumption.

The heater in this experiment can represent for example overheating following intense physical activity. For a temperature difference $\Delta T = 6$ K and a flow rate $Q = 100$ µl/s, we can estimate a heat transport ability of 1.1 W, one order of magnitude higher than the power consumption of the pump (~0.1 W), showing its effectiveness as a wearable thermal regulation device. The experimental results shown in Fig. 3 confirm this estimation, as the pump transports the heat away from an overheated body area to the periphery (Supplementary Video 3). More information on the thermal regulation experiments can be found in the Methods section. Thanks to its small size, compliance and low-weight, the stretchable pump does not interfere with the physical movements, paving the way for wearable fluidic circuits for thermal regulation constituted by multiple pumps which could be integrated in everyday clothing, sportswear or wearable protections for severe environments.

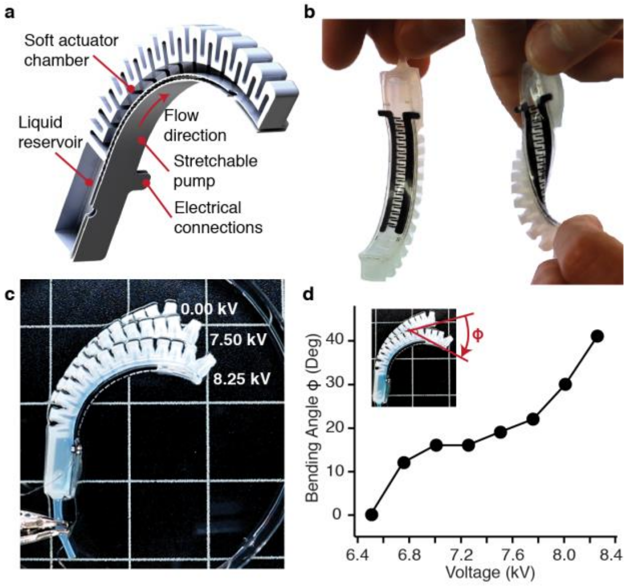

Fig. 4: Fluidic muscles obtained by bonding a stretchable pump to a bending fluidic actuator. **a**, Schematic longitudinal cross section of the fluidic muscle, showing the main components. The inlet of the pump is connected to a small reservoir at the back of the actuator, while the outlet is connected to the bellows-shaped bending chamber. **b**, The entire actuator is soft and can be easily deformed. **c**, Once pre-filled with dielectric liquid, the actuator does not have any external tubing. It bends when a voltage is applied: the soft pump moves the liquid from the reservoir to the bending chamber, producing its deformation. **d**, Measured bending angle as a function of the applied voltage. Supplementary Video 4 shows the fluidic muscle in action.

We then considered the integration of the stretchable pumps in fluidic actuators, which are often used in combination with conventional rigid pumps or compressors. Figure 4 shows a fluidic muscle composed of a bending fluidic actuator[7] with a stretchable pump embedded in its bottom layer. The pump pushes liquid from a small reservoir in the back of the actuator to a bellows-shaped chamber, whose inflation causes bending of the actuator. When the voltage is applied, the actuator bends by over 40° relative to its rest position (Fig. 4c-d and Supplementary Video 4). Figure 4d shows the fluidic muscle's angle vs. voltage curve, whose shape results from a combination of the nonlinear response of bending fluidic actuators and that of the soft pump (Fig. 2c). When the voltage is removed, the fluidic muscle returns to its initial position thanks to the restoring elastic forces of the chamber. Such actuators are promising building block for the next generation of soft robots, combining the robustness, large deformation and versatility of fluidic actuators with the portability of an integrated system that does not require external compressors.

METHODS

ElectroHydroDynamics (EHD) pumping principle

EHD pumping refers to the acceleration of a fluid by means of an electric field[19]. In this work, we explored two EHD pumping mechanisms.

The first mechanism (Extended Data Fig. 1a) is called conduction pumping and relies on the formation of heterocharge layers in the proximity of the electrodes[21]. Heterocharge layers are non-equilibrium charged layers that form when the electric field exceeds a certain threshold ($5 - 6\ \mathrm{V/\mu m}$) due to ion generation not balanced by recombination. The charges in these layers are of opposite sign to that of the adjacent electrode, thus they are electrostatically pulled towards the electrode, where they discharge. The movement of ions, which drags the neutral liquid molecules and thus generates pumping, is identical at the anode and at the cathode. As a consequence, to obtain global flow (i.e., not simply local recirculation) the electrodes surface must be oriented such that the direction normal to the electrodes has a non-zero component oriented in the direction of the desired flow. The flow direction is therefore determined by the design of the electrodes and not by the field polarity. This conduction pumping mechanism consists of an array of inclined capacitors obtained by overlapping symmetrical electrodes on an inclined channel, as shown in Extended Data Fig. 1a.

The second mechanism (Extended Data Fig. 1b) is called charge injection and is based on field emission[20,22]. When the electric field is high enough, electrons can overcome the energy barrier and directly tunnel from the cathode surface into the dielectric liquid. The ions thus formed are accelerated by the electrophoretic force until they discharge at the anode. The use of dielectric liquids with highly electronegative molecules (e.g., fluorine-based liquids) ensures that the energy barrier for field emission to occur at the cathode is significantly lower than at the anode. This mechanism can create net flow with a planar electrodes configuration and a DC electric field. The flow direction can be inverted by inverting the polarity of the electric field. Extended Data Fig. 1b shows the design of the soft pump based on injection pumping, consisting of two overlapped sets of interdigitated electrodes.

In both mechanisms, once one has exceeded the electric field threshold needed for the phenomenon to occur, the pumping pressure Δp grows with the square of the electric field and linearly with the dielectric constant of the liquid: $\Delta p = k_p \varepsilon E^2$, where k_p is a constant depending on the pump geometry. The generated flow-rate Q has a more complicated relation; it generally depends on the electric field squared and on the fourth power of the channel size D: $Q = k_Q \varepsilon E^2 D^4$. The direction of the flow is opposite to the direction of the electric field for charge injection, while it depends only on the geometry of the electrodes for conduction pumping.

One has a great deal of design freedom for the EHD electrode configurations. For the interdigitated case, one can reduce the inter-electrode distance g to simultaneously lower the drive voltage for a given electric field and to increase the number of electrode pairs (hence pressure) in a given channel length. How the inter-electrode gap influences pressure and flow rate is non-trivial: a smaller gap spacing leads to electric field lines that penetrate less far into the channel, thus dragging ions along a thinner sheath. Increasing the width of the electrodes will proportionally increase flow rate. Scaling down ever further leads to lower voltages but creates a flow only very near to the wall, with much higher friction losses. We propose that a gap of order channel thickness is a reasonable starting point.

Dielectric fluids for EHD pumping must have low electrical conductivity ($<10^{-7}$ S/m) and high electrical breakdown strength to enable high pumping pressure. Of the different liquids one can consider, Novec 7100 and Fluorinert FC40 both have excellent dielectric strength, with nominal breakdown voltages of 10-16 kV and > 18 kV for 1 mm gaps, respectively. The boiling points of Novec 7100 and Fluorinert FC40 are 61 °C and 155 °C, making them well-suited for room temperature operation. Both fluids have very low toxicity, zero ozone depletion potential, no flash point and are nonflammable.

Stretchable pumps: four generations

We designed and developed four generations of stretchable pumps (Extended Data Fig. 3). The circuit of the first generation ("inclined 1", see Extended Data Fig. 1a) consists of a set of 5 inclined capacitors (corresponding to 10 electrode units) separated by a 1 mm gap. It operates according to EHD conduction pumping principles. The second generation (inclined 2) is a scaled down version of the first one with half the channel size, half the electrode gap, and 43 inclined capacitors (86 electrode units).

The third generation (C pump) relies on the charge injection mechanism (Extended Data Fig. 1b) and thus presents a different electrode layout: two series of 17 interdigitated electrodes facing each other (68 electrode units). The fourth generation (Ag pump) has the same geometry as the third one but the electrode material has been replaced by a commercial silver ink. The reason for this materials change is the degradation observed in the performance of carbon-based electrodes, which is completely solved by using silver particles as a conductive material.

The inclined design presents lower pumping performance for the same applied voltage compared to the interdigitated design, as shown in Extended Data Fig. 3. Additionally, the interdigitated design allows pumping in either direction, based on the polarity of the applied voltage, while the inclined design always generates flow according to the gradient in the electric field (from the larger gap side to smaller gap side). However, the conduction pumping mechanism is less subject to electrodes deterioration than the charge injection used in the interdigitated design[19,21,22]. Another advantage of the inclined design over the interdigitated one is robustness to minor electrical breakdown events. In the inclined design, the short-circuit path between electrodes with opposite polarity is always through the dielectric liquid, so permanent short circuits do not form, as in HASEL actuators[12]. On the contrary, in the interdigitated design, conductive paths can form on the PDMS substrate rather than through the liquid, preventing the healing of the device.

A comparison between the inclined 1 and inclined 2 designs shows the scalability of the stretchable pumps both in terms of channel size and electrodes spacing. By varying the channel height, which in this configuration corresponds to the gap between the electrode pairs (Extended Data Fig. 1a), we change the electric field at a given voltage. As a consequence, the response of the inclined 1 pump is shifted to double the voltages of the inclined 2, as we would expect since the EHD phenomenon depends on the value of the electric field. We can also observe a direct proportionality between the number of electrode pairs and the generated pressure.

Materials and Fabrication

The stretchable pumps are composed of two electrode layers that sandwich a channel layer. The Polydimethylsiloxane (PDMS) used for the pump body is Dow Corning Sylgard 184. The electrode layers are symmetric and are patterned on a 0.4 mm thick PDMS backing. The electrode material for the C pumps is composed of carbon particles dispersed in a soft PDMS matrix[32] (Silbione LSR 4305), while for the Ag pumps the electrode is printed using a commercially-available stretchable silver ink (Chimet Ag 520 EI) using a laser-engraved Mylar (BoPET, Biaxially-oriented polyethylene terephthalate) mask. The channel layer consists of a laser-cut PDMS membrane, whose thickness determines the height of the channel (1.0 mm or 0.5 mm in the devices we developed). The layers are bonded using a silicone adhesive film (AR Clear 8932EE, Adhesives Research), which is laminated on the channel layer before the laser cutting process. Extended Data Fig. 2 shows the details of the fabrication process. The dielectric liquids used for the stretchable pumps are fluorinated solvents: 3M Novec 7100, methoxy-nonafluorobutane ($C_4F_9OCH_3$) for the C pumps, and 3M Fluorinert FC-40 ($C_{10}HF_{22}N$) for the Ag pumps.

Characterization experiments

Pressure and flow-rate measurements were performed using the pumps in a closed loop with a variable-opening valve to control the fluidic impedance. The pumps were powered using power supplies based on the Peta-Pico-Voltron[33] (https://petapicovoltron.com/) open source HV supply for voltages up to 5 kV, and using an EMCO regulated CB101 up to 10 kV. The applied voltage, electrical current, pressure and flow-rate were simultaneously recorded.

The Ag devices operate stably in air with no special pre-treatment: we routinely operated the Ag pumps in lab ambient for several hours. For the C pumps however, most characterization experiments were conducted with the stretchable pumps submerged in the same dielectric liquid used for pumping (3M Novec 7100), as operating in liquid allows for long-term testing for the C pumps. PDMS is permeable to, and swells in, Novec 7100; operating in air eventually results in gas bubbles inside the channel. Soaking the device in Novec 7100 temporarily prevented gas formation and allowed reliable operation in air for up to 15 min.

The thermal regulation and soft robotic actuator experiments were carried with C pumps in air after soaking the pump in the dielectric liquid for 10-15 min.

Heart-shaped balloon

The heart-shaped balloon consists of two separate fluidic chambers (ventricles). It is manufactured by mold casting a soft silicone rubber (Smooth-on Ecoflex 0030) in a CNC-machined plastic mold and then gluing this molded body to a 100 µm thick membrane made with the same silicone. Each side of a stretchable pump is connected to one of the two ventricles of the balloon using small vinyl tubes (1.2 mm ID). Before each experiment, the circuit is pre-filled with dielectric liquid (FC-40) and most of the air is removed. The voltage is applied to the pump using a battery-driven high-voltage power supply (Extended Data Fig. 4). Based on the polarity of the applied voltage, the pump moves the liquid from the left ventricle to the right one or vice-versa (Fig. 1d, Supplementary Video 2). In this experiment, we used a modified version of the Ag pump, where the gap between the interdigitated electrodes has been reduced from 0.5 mm to 0.4 mm to increase the electric field for the same applied voltage and comply with the maximum 6 kV output of the battery-driven power supply.

Thermal regulation on a smart glove

In this experiment, the fluid circulation driven by a stretchable pump transfers heat between a hot area and a cold one. To a first approximation, the rate of heat transfer H in a fluidic heat exchanger is proportional to the flow-rate Q, according to the equation $H = Q\rho c_p \Delta T$, where $c_p = 1183\ \mathrm{J/kg/K}$ is the specific heat of our working fluid (Novec 7100), $\rho = 1510\ \mathrm{kg/m^3}$ its density and ΔT the temperature difference between the inlet and the outlet of the exchanger. The rate of heat transfer H, measured in watts, represents the amount of thermal power that can be transported by the fluid.

The hot area in our set-up is represented by a flexible joule heater (MINCO polyimide thermofoil heater) while the cold one by a serpentine sewed in a textile glove, where the heat can be dissipated by natural air convection. The closed-loop fluidic circuit is filled with dielectric liquid and air bubbles are removed before activating the pump. We apply a constant voltage of 9V on the heater, leading to a thermal power of 1.2 W. The temperature map is acquired using an IR camera (FLIR A15, 50 mK thermal sensitivity). The emissivity is set to a constant value of 0.98, given the very similar values of emissivity of all the materials involved in the set-up (i.e., human skin, elastomers, plastic foils).

Soft robotic actuator

The bending fluidic actuator is manufactured by mold casting a soft silicone rubber (Smooth-on Ecoflex 0030) in a 3D printed mold[7]. Pump and actuator are bonded together, fluidically connected and sealed using a silicone glue (Wacker Silpuran 4200). The experiment is conducted with the soft actuator lying on a horizontal plane lubricated with Novec 7100 to prevent stiction. Before starting the experiment, the actuator is filled with dielectric liquid using the tube in its back. Air bubbles are evacuated using gravity. The actuator reservoir is filled with dielectric liquid and the actuators takes a curved shape at rest due to the liquid pressure. This pressure causes the pump channel to expand slightly, resulting in slightly higher pump working voltages compared to the uninflated case. The bending is recorded with a camera and the angle computed using Kinovea software for image analysis.

Data availability

All data are available from the corresponding authors upon reasonable request.

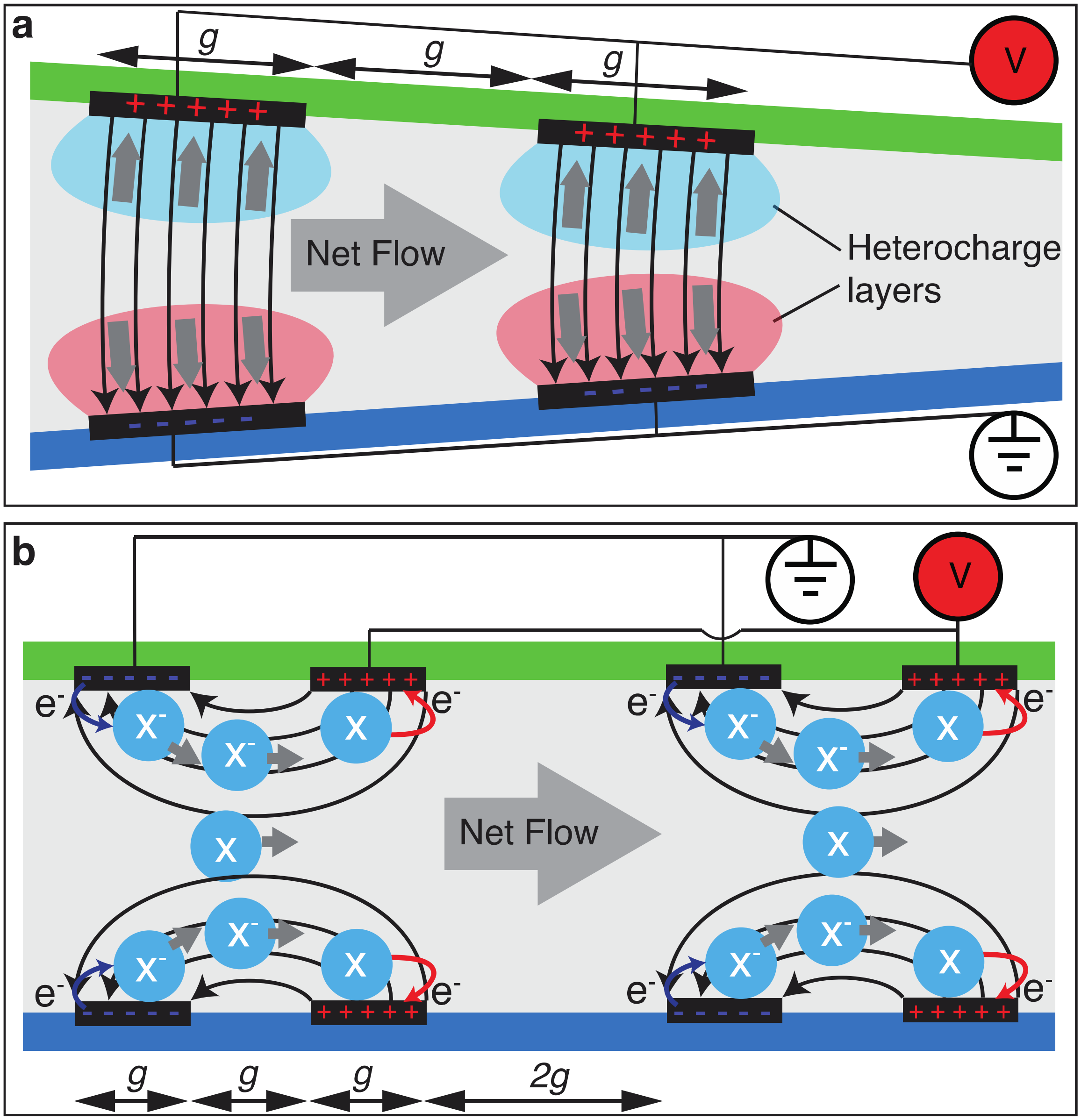

Extended Data Figure 1: The two different electrode geometries and corresponding ElectroHydroDynamic (EHD) mechanisms used in this work.

a, Conduction pumping, with inclined capacitors. Heterocharge layers form in the proximity of the electrodes. These layers are characterized by a higher concentration of ions of opposite polarity with respect to the opposing electrode. As a consequence, these ions are attracted to the opposite electrode, where they discharge. The inclined capacitors geometry allows net flow thanks to the in-flow component of the electric field in proximity of the electrodes surface. **b**, Charge injection, with interdigitated electrodes. When the electric field is high enough to overcome the energy barrier, field emission takes place, with electrons tunneling from the cathode into the dielectric liquid. The generated ions are accelerated by the electric field until they discharge at the anode, transferring momentum to neutral liquid molecules along the way.

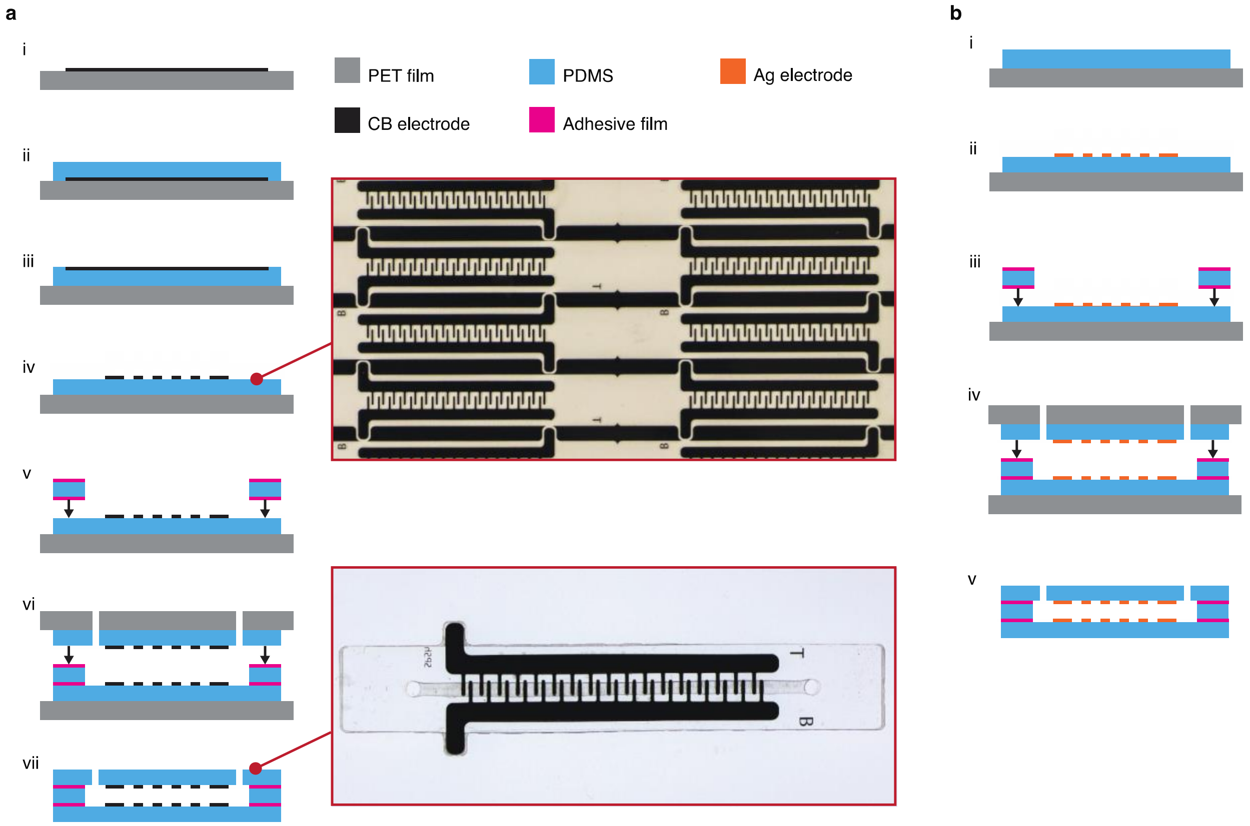

Extended Data Figure 2: Fabrication process for the stretchable pumps using the interdigitated design.

a, Fabrication process of the C pump. (i) The fabrication of the electrode layers starts by blade casting a carbon-based electrode membrane with a thickness of 30 µm on a PET support, which is then cured at 80 °C for 2 h. (ii) A 400 µm PDMS membrane is casted on the top of the electrode and cured at 80 °C for 1 h. (iii) The sample is turned over in order to expose the electrode membrane, (iv) which is then processed by laser engraving to define the interdigitated pattern. This process allows the manufacturing of many samples in parallel (up to 24 samples with our equipment at EPFL-LMTS). (v) The channel layer, consisting of a 500 µm thick laser-cut PDMS membrane, is bonded on the bottom electrode layer using a silicone adhesive film. (vi) The top electrode layer, having two laser-cut holes for fluidic connection, is finally bonded on the top of the channel layer. (vii) The PET supports are removed and the C stretchable pumps are ready to use. **b,** Fabrication process of the Ag pump. (i) The fabrication starts by blade casting and curing (80 °C, 1h) a 400 µm PDMS membrane. (ii) On the PDMS, a silver-based stretchable ink is printed through a 23 µm thick Mylar mask and cured at 80 °C for 3 h. (iii) After removing the mask, the bottom electrode layer is bonded to the 500 µm thick channel layer using a silicone adhesive film. (iv) The top electrode layer, having two laser-cut holes for fluidic connection, is finally bonded on the top of the channel layer. (v) The PET supports are removed and the Ag stretchable pumps are ready to use.

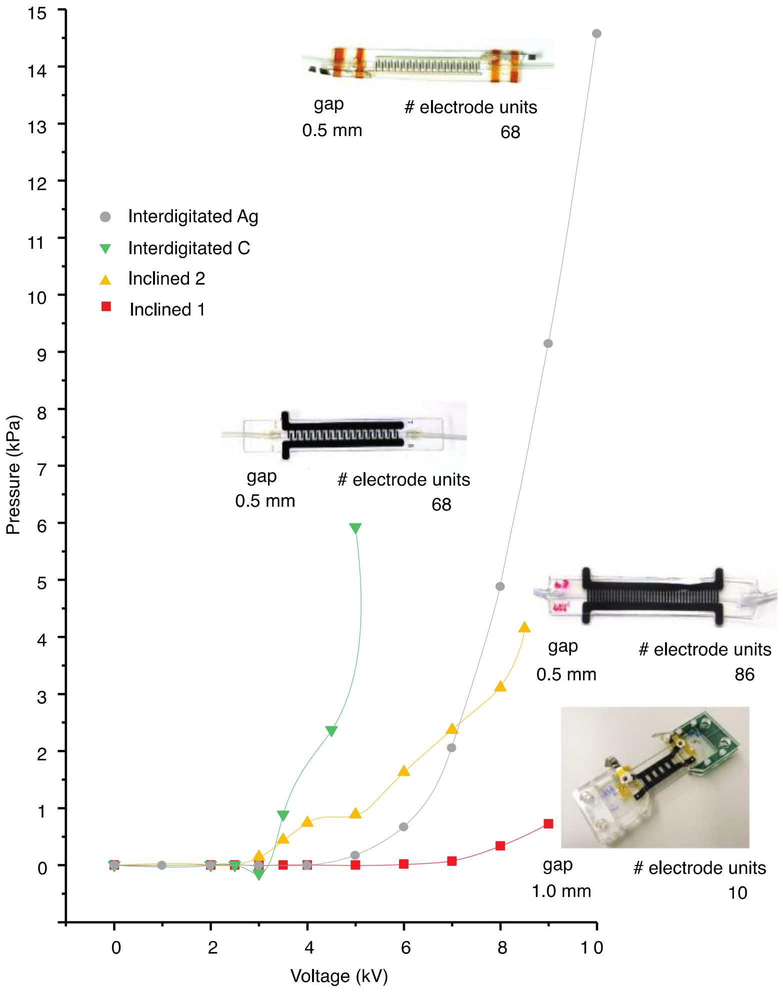

Extended Data Figure 3: Four generations of stretchable pumps plotting generated pressure vs. applied voltage.
The “inclined 1” and “inclined 2” generations have inclined capacitors as the electrode configuration. “inclined 2” is a scaled version of “inclined 1”, with half the channel size, half the gap between opposite electrodes, and 8.6 times more electrode pairs. The interdigitated generations have the same channel size and gap between opposite electrodes as “inclined 2”, but use interdigitated electrodes rather than inclined capacitors. The C version has laser-engraved carbon-silicone composite electrodes and uses 3M Novec 7100 as the dielectric fluid, while the Ag version has mask-printed silver-based electrodes and uses 3M Fluorinert FC-40 as the dielectric fluid. The Ag devices can sustain higher fields than the C devices thanks to the different dielectric liquid and to the different electrode fabrication method.

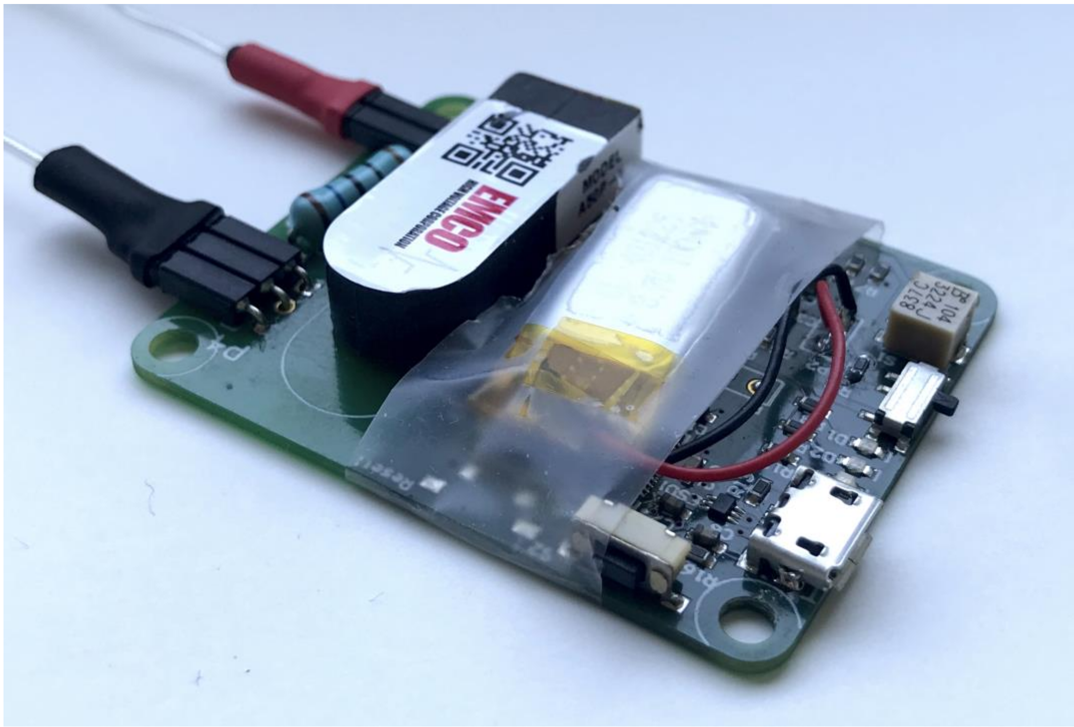

Extended Data Figure 4: A 5 kV programmable power supply weighing 16 g, including Li-ion battery.

This custom-made power supply is based on an EMCO DC-DC converter from XP-power (https://www.xppower.com/Product/A-Series) and includes a microcontroller to program the output. Dimensions are 5 cm × 4 cm × 0.8 cm. In this work we also used a 6 kV, 20 g version.

Extended Data Figure 5: Three stretchable pumps connected in series.
The data shown in Fig. 2f were taken using these three pumps connected in series to increase pressure. Alternatively, pumps could be connected in parallel for higher flow rate. Each pump is 7.5 cm long.

Concise overview of miniature pump performance

Table 1 below compares performance of pumps based on a broad range of physical principles, as reviewed in [20,30,31]. Some numbers, pump overall volume in particular, are approximate because authors include different elements when reporting pump dimensions, in part due the large range of possible actuation methods.

Our stretchable pump significantly surpasses all reported soft pumps in both specific pressure and specific flow rate.

Amongst published soft pumps, combustion-driven pumps provide the highest absolute pressure and flow rates, but require a source of combustible gas, an ignition system, and a design that can tolerate the high combustion temperatures and pressure bursts. Those pumps can be challenging to regulate and are mostly adapted to generate explosive motion such as for jumping robots. Electroosmotic pumps are in principle well-suited to fabrication in a stretchable format given their simple structure. The one reported stretchable device is fabricated with extremely small micromachined channels, leading to very low flow rates, far too small for soft robotics or wearable applications. Pneumatic actuation allows for ready use of soft materials, but the need for an external source of compressed air is impractical for the applications we report in this paper.

Extended Data Table 1: Pump performance comparison

Category	Reference	Pumping Principle	Approximate Size (cm^3)[*]	Max. Power Consumption (W)	Max. pressure (kPa)	Max. Flow Rate (ml/min)	Max. Power Consumption / Size (× 10 kW/m^3)	Pressure / Size (GPa/m^3)	Flow Rate Size (x10^3 l/min/
Stretchable pumps									
	This study	Electrohydro-dynamic	1.17	0.17	14	6.0	14.5	12	5.13
Commercial pumps									
	High performance miniature pump (MGD 1000S)[34]	Electromagnetic	58.6	30	800	500	51.2	13.7	8.5
	Off-the-shelf compressor (McMaster STPAC)[35]	Electromagnetic	75500	1200	1034	42500	1.59	0.01	0.56
Micropumps[†]									
	36	Piezoelectric	0.26	N/A	74	1.1	N/A	284	4.2
	37	Piezoelectric	1.98	0.4	0.52	0.04	20.2	0.26	0.02
	38	Electromagnetic	3.5	0.17	8	9.5	4.86	2.29	2.71
	39	Electromagnetic	50.6	N/A	25.5	0.14	N/A	0.5	0.003
	40	Electrohydro-dynamic	0.01[‡]	N/A	1.75	14	N/A	175	1400
	41	Electrohydro-dynamic	0.09[‡]	0.35	0.25	0.04	389	2.78	0.44
	42	Electroosmotic	0.04[‡]	0.88	10000	0.002	2200	250000	0.05
	43	Electroosmotic	9	0.002	33	0.02	0.02	3.67	0.002
	44	Electrostatic	0.1	N/A	29	0.16	N/A	290	1.6
	45	Piezoelectric	0.26	N/A	74	1.1	N/A	284	4.2
	46	Magnetohydro-dynamic	2.03	N/A	0.75	0.7	N/A	0.37	0.25
	47	Ionic	0.8	N/A	0.17	0.005	N/A	0.21	0.001
	48	Thermo-pneumatic	3	N/A	5.1	0.03	N/A	1.7	0.01
	49	Phase change	0.07	N/A	0.1	0.006	N/A	1.43	0.086
	50	Thermo-pneumatic	0.004[‡]	3.4	0.49	0.01	85000	123	2.5
	51	Pneumatic	6	N/A	0.44	0.09	N/A	0.07	0.15
Pumps using soft or flexible materials									
	52	Thermo-pneumatic	11	N/A	3.5	0.02	N/A	0.32	0.002
	53	Electroosmotic	0.01[‡]	N/A	0.01	0.001	N/A	1	0.1
	54	Combustion	49	N/A	60	40	N/A	1.22	0.82
	55	Pneumatic	500 (estimated from photo)	N/A	20	430	N/A	0.04	0.86
	56	Combustion	314	N/A	130	240	N/A	0.41	0.76

[*] Volume based on data in paper, photographs/figures. We attempted to include the same key components in each pump for a fair comparison, despite importa differences in fabrication methods and in operating principles.

[†] Reference selected from review articles 20,30,31. Some numbers differ from review article following analysis of the papers.

[‡] Channel or chamber dimensions, no data available on full pump.

REFERENCES

1. Rus, D. & Tolley, M. T. Design, fabrication and control of soft robots. *Nature* **521**, 467–475 (2015).
2. Laschi, C., Mazzolai, B. & Cianchetti, M. Soft robotics: Technologies and systems pushing the boundaries of robot abilities. *Science Robotics* **1**, (2016).
3. Amjadi, M., Kyung, K.-U., Park, I. & Sitti, M. Stretchable, Skin-Mountable, and Wearable Strain Sensors and Their Potential Applications: A Review. *Advanced Functional Materials* **26**, 1678–1698 (2016).
4. Hines, L., Petersen, K., Lum, G. Z. & Sitti, M. Soft Actuators for Small-Scale Robotics. *Advanced Materials* **29**, 1603483 (2017).
5. Suzumori, K., Iikura, S. & Tanaka, H. Development of flexible microactuator and its applications to robotic mechanisms. in *1991 IEEE International Conference on Robotics and Automation Proceedings* 1622–1627 vol.2 (1991).
6. Suzumori, K., Wada, A. & Wakimoto, S. New mobile pressure control system for pneumatic actuators, using reversible chemical reactions of water. *Sensors and Actuators, A: Physical* **201**, 148–153 (2013).
7. Polygerinos, P. *et al.* Soft Robotics: Review of Fluid-Driven Intrinsically Soft Devices; Manufacturing, Sensing, Control, and Applications in Human-Robot Interaction. *Advanced Engineering Materials* **19**, 1700016 (2017).
8. Shintake, J., Cacucciolo, V., Floreano, D. & Shea, H. Soft Robotic Grippers. *Advanced Materials* **30**, 1707035 (2018).
9. Keplinger, C. *et al.* Stretchable, Transparent, Ionic Conductors. *Science* **341**, 984–987 (2013).
10. Viry, L. *et al.* Flexible Three-Axial Force Sensor for Soft and Highly Sensitive Artificial Touch. *Advanced Materials* **26**, 2659–2664 (2014).
11. Rosset, S. & Shea, H. R. Small, fast, and tough: Shrinking down integrated elastomer transducers. *Applied Physics Reviews* **3**, 031105 (2016).
12. Acome, E. *et al.* Hydraulically amplified self-healing electrostatic actuators with muscle-like performance. *Science* **359**, 61–65 (2018).
13. Dong, L., Agarwal, A. K., Beebe, D. J. & Jiang, H. Adaptive liquid microlenses activated by stimuli-responsive hydrogels. *Nature* **442**, 551–554 (2006).
14. Rossiter, J., Takashima, K., Scarpa, F., Walters, P. & Mukai, T. Shape memory polymer hexachiral auxetic structures with tunable stiffness. *Smart Mater. Struct.* **23**, 045007 (2014).

15. Majidi, C., Kramer, R. & Wood, R. J. A non-differential elastomer curvature sensor for softer-than-skin electronics. *Smart Mater. Struct.* **20**, 105017 (2011).

16. Cooper, C. B. *et al.* Stretchable Capacitive Sensors of Torsion, Strain, and Touch Using Double Helix Liquid Metal Fibers. *Advanced Functional Materials* **27**, 1605630 (2017).

17. Pan, C. *et al.* Visually Imperceptible Liquid-Metal Circuits for Transparent, Stretchable Electronics with Direct Laser Writing. *Advanced Materials* **30**, 1706937 (2018).

18. Besse, N., Rosset, S., Zarate, J. J. & Shea, H. Flexible Active Skin: Large Reconfigurable Arrays of Individually Addressed Shape Memory Polymer Actuators. *Advanced Materials Technologies* **2**, 1700102 (2017).

19. Ramos, A. *Electrokinetics and Electrohydrodynamics in Microsystems*. (Springer Vienna, 2011).

20. Iverson, B. D. & Garimella, S. V. Recent advances in microscale pumping technologies: A review and evaluation. *Microfluidics and Nanofluidics* **5**, 145–174 (2008).

21. Pearson, M. & Seyed-Yagoobi, J. Advances in electrohydrodynamic conduction pumping. *IEEE Transactions on Dielectrics and Electrical Insulation* **16**, 424–434 (2009).

22. Darabi, J. & Wang, H. Development of an electrohydrodynamic injection micropump and its potential application in pumping fluids in cryogenic cooling systems. *Journal of Microelectromechanical Systems* **14**, 747–755 (2005).

23. Chang, S. T., Paunov, V. N., Petsev, D. N. & Velev, O. D. Remotely powered self-propelling particles and micropumps based on miniature diodes. *Nature Materials* **6**, 235–240 (2007).

24. Kim, J. W., Suzuki, T., Yokota, S. & Edamura, K. Tube-type micropump by using electro-conjugated fluid (ECF). *Sensors and Actuators, A: Physical* **174**, 155–161 (2012).

25. Cacucciolo, V., Shigemune, H., Cianchetti, M., Laschi, C. & Maeda, S. Conduction Electrohydrodynamics with Mobile Electrodes: A Novel Actuation System for Untethered Robots. *Advanced Science* 1600495 (2017).

26. Wehner, M. *et al.* Pneumatic Energy Sources for Autonomous and Wearable Soft Robotics. *Soft Robotics* **1**, 263–274 (2014).

27. Rosset, S. & Shea, H. R. Flexible and stretchable electrodes for dielectric elastomer actuators. *Appl. Phys. A* **110**, 281–307 (2013).

28. Shintake, J., Rosset, S., Schubert, B., Floreano, D. & Shea, H. Versatile Soft Grippers with Intrinsic Electroadhesion Based on Multifunctional Polymer Actuators. *Advanced Materials* **28**, 231–238 (2016).

29. Wehner, M. *et al.* An integrated design and fabrication strategy for entirely soft, autonomous robots. *Nature* **536**, 451–455 (2016).

30. Laser, D. J. & Santiago, J. G. A review of micropumps. *Journal of Micromechanics and Microengineering* **14**, R35–R64 (2004).

31. Wang, Y.-N. & Fu, L.-M. Micropumps and biomedical applications – A review. *Microelectronic Engineering* **195**, 121–138 (2018).

ADDITIONAL REFERENCES

32. Rosset, S., Araromi, O. A., Schlatter, S. & Shea, H. R. Fabrication Process of Silicone-based Dielectric Elastomer Actuators. *Journal of Visualized Experiments* 1–13 (2016).
33. Schlatter, S., Illenberger, P. & Rosset, S. Peta-pico-Voltron: An open-source high voltage power supply. *HardwareX* **4**, e00039 (2018).
34. MGD 1000S. Available at: https://www.micropumps.co.uk/TCSMGD1000range.htm.
35. McMaster STPAC. Available at: https://www.mcmaster.com/9965k62.
36. Olsson, A., Enoksson, P., Stemme, G. & Stemme, E. Micromachined flat-walled valveless diffuser pumps. *Journal of Microelectromechanical Systems* **6**, 161–166 (1997).
37. Jang, L.-S. *et al.* A stand-alone peristaltic micropump based on piezoelectric actuation. *Biomed Microdevices* **9**, 185–194 (2007).
38. Lei, K. F. *et al.* A vortex pump-based optically-transparent microfluidic platform for biotech and medical applications. *Proc Inst Mech Eng H* **221**, 129–141 (2007).
39. Kawun, P., Leahy, S. & Lai, Y. A thin PDMS nozzle/diffuser micropump for biomedical applications. *Sensors and Actuators A: Physical* **249**, 149–154 (2016).
40. Richter, A., Plettner, A., Hofmann, K. A. & Sandmaier, H. A micromachined electrohydrodynamic (EHD) pump. *Sensors and Actuators A: Physical* **29**, 159–168 (1991).
41. Ahn, S.-H. & Kim, Y.-K. Fabrication and experiment of a planar micro ion drag pump. *Sensors and Actuators A: Physical* **70**, 1–5 (1998).
42. Chen, L., Wang, H., Ma, J., Wang, C. & Guan, Y. Fabrication and characterization of a multi-stage electroosmotic pump for liquid delivery. *Sensors and Actuators, B: Chemical* **104**, 117–123 (2005).
43. Chuan-Hua Chen & Santiago, J. G. A planar electroosmotic micropump. *Journal of Microelectromechanical Systems* **11**, 672–683 (2002).
44. Zengerle, R., Ulrich, J., Kluge, S., Richter, M. & Richter, A. A bidirectional silicon micropump. *Sensors and Actuators A: Physical* **50**, 81–86 (1995).
45. Homsy, A., Linder, V., Lucklum, F. & de Rooij, N. F. Magnetohydrodynamic pumping in nuclear magnetic resonance environments. *Sensors and Actuators B: Chemical* **123**, 636–646 (2007).
46. Ashouri, M., Shafii, M. B. & Moosavi, A. Theoretical and experimental studies of a magnetically actuated valveless micropump. *J. Micromech. Microeng.* **27**, 015016 (2016).

47. Tanaka, Y., Noguchi, Y., Yalikun, Y. & Kamamichi, N. Earthworm muscle driven bio-micropump. *Sensors and Actuators B: Chemical* **242**, 1186–1192 (2017).

48. Van de Pol, F. C. M., Van Lintel, H. T. G., Elwenspoek, M. & Fluitman, J. H. J. A thermopneumatic micropump based on micro-engineering techniques. *Sensors and Actuators A: Physical* **21**, 198–202 (1990).

49. Sim, W. Y., Yoon, H. J., Jeong, O. C. & Yang, S. S. A phase-change type micropump with aluminum flap valves. *J. Micromech. Microeng.* **13**, 286–294 (2003).

50. Jung, J.-Y. & Kwak, H.-Y. Fabrication and testing of bubble powered micropumps using embedded microheater. *Microfluid Nanofluid* **3**, 161–169 (2007).

51. Shaegh, S. A. M. *et al.* Plug-and-play microvalve and micropump for rapid integration with microfluidic chips. *Microfluid Nanofluid* **19**, 557–564 (2015).

52. Jeong, O. C., Park, S. W., Yang, S. S. & Pak, J. J. Fabrication of a peristaltic PDMS micropump. *Sensors and Actuators A: Physical* **123–124**, 453–458 (2005).

53. Jahanshahi, A., Axisa, F. & Vanfleteren, J. Fabrication of an implantable stretchable electro-osmosis pump. in *Microfluidics, BioMEMS, and Medical Microsystems IX* **7929**, 79290R (International Society for Optics and Photonics, 2011).

54. Stergiopulos, C., Vogt, D., Tolley, M. & Wehner, M. a Soft Combustion-Driven Pump for Soft Robots. *Proceedings of the ASME 2014 Conference on Smart Materials, Adaptive Structures and Intelligent Systems SMASIS2014* 1–6 (2014).

55. Murray, B. C. M. *et al.* Poroelastic Foams for Simple Fabrication of Complex Soft Robots. *Advanced Materials* **27**, 6334–6340 (2015).

56. Loepfe, M., Schumacher, C. M. & Stark, W. J. Design, Performance and Reinforcement of Bearing-Free Soft Silicone Combustion-Driven Pumps. *Ind. Eng. Chem. Res.* **53**, 12519–12526 (2014).

Acknowledgments: We are grateful to H. Shigemune for discussions about EHD, to M. Imboden for assistance with the thermal regulation experiments, and to O. Gudozhnik for developing the 5 and 6 kV supply weighing 16-20 g. We acknowledge financial support from JSPS KAKENHI under Grants 16H04306, 18H05473, and 19H05328; MEXT/JSPS under Leading Initiative for Excellent Young Researchers; Swiss National Science Foundation through NCCR Robotics; Japanese TOBITATE! Young Ambassador Program; Hasler Foundation Cyber-Human Systems program; the BioRobotics Institute of Scuola Superiore Sant'Anna, Pisa in the person of Cecilia Laschi for Vito Cacucciolo's initial visit to EPFL.

Author contributions: V.C., J.S., S.M., D.F., and H.S. conceived the project. V.C. and J.S. designed and characterised the devices. V.C., J.S. and Y.K. fabricated the devices. V.C. and H.S. analysed the data. S.M., H.S. and D.F. contributed to data interpretation. V.C., J.S. and H.S. wrote the paper. All authors provided feedback and agree with the final version of the manuscript.

The authors declare the following competing financial interest(s): V.C., J.S., S.M., D.F., and H.S declare financial interest in form of a patent application.